

Conducting MoS₂ Nanosheets as Catalysts for Hydrogen Evolution Reaction

Damien Voiry,[†] Maryam Salehi,[†] Rafael Silva,[‡] Takeshi Fujita,^{§,||} Mingwei Chen,[§] Tewodros Asefa,^{‡,⊥} Vivek B. Shenoy,[#] Goki Eda,^{∇,○} and Manish Chhowalla*,[†]

[†]Materials Science and Engineering, Rutgers University, 607 Taylor Road, Piscataway, New Jersey 08854, United States

[‡]Department of Chemistry and Chemical Biology, Rutgers University, 610 Taylor Road, Piscataway, New Jersey 08854, United States

[§]WPI Advanced Institute for Materials Research, Tohoku University, Sendai 980-8577, Japan

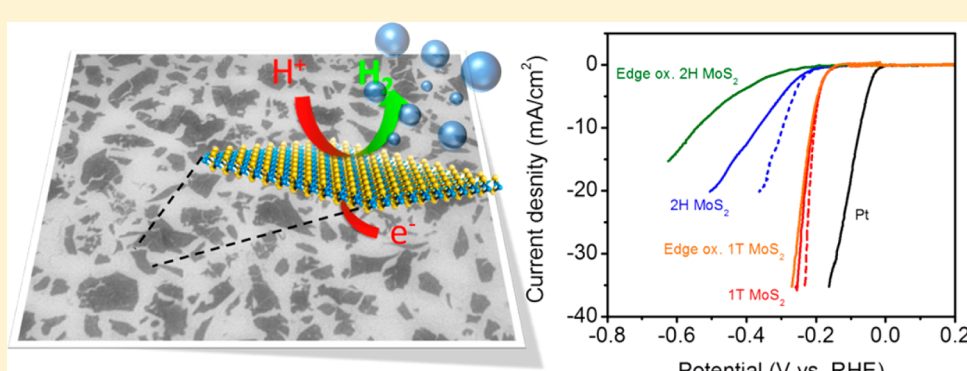
^{||}JST, PRESTO, 4-1-8 Honcho Kawaguchi, Saitama 332-0012, Japan

[#]Department of Chemical and Biochemical Engineering, Rutgers University, 98 Brett Road, Piscataway, New Jersey 08854, United States

[∇]Physics Department and Graphene Research Centre, National University of Singapore, 2 Science Drive 3, Singapore 117542

[○]Chemistry Department, National University of Singapore, 3 Science Drive 3, Singapore 117543

Supporting Information



ABSTRACT: We report chemically exfoliated MoS₂ nanosheets with a very high concentration of metallic 1T phase using a solvent free intercalation method. After removing the excess of negative charges from the surface of the nanosheets, highly conducting 1T phase MoS₂ nanosheets exhibit excellent catalytic activity toward the evolution of hydrogen with a notably low Tafel slope of 40 mV/dec. By partially oxidizing MoS₂, we found that the activity of 2H MoS₂ is significantly reduced after oxidation, consistent with edge oxidation. On the other hand, 1T MoS₂ remains unaffected after oxidation, suggesting that edges of the nanosheets are not the main active sites. The importance of electrical conductivity of the two phases on the hydrogen evolution reaction activity has been further confirmed by using carbon nanotubes to increase the conductivity of 2H MoS₂.

KEYWORDS: Layered materials, MoS₂, chemical exfoliation, layered transition metal dichalcogenide, hydrogen evolution reaction

Hydrogen is the cleanest fuel and represents one of the most promising energy sources.¹ Efficient hydrogen evolution using metal alloy,^{2,3} enzyme,⁴ metal oxides,^{5,6} metal dichalcogenides,⁷ and bioinspired molecular electrocatalysts^{8–10} has been reported. The identification of catalytic activity from edges of MoS₂ crystals has led to numerous studies related to hydrogen evolution reaction (HER)^{11,12} using non-metallic, inexpensive, and earth abundant catalysts. This approach has focused on enhancing the edge concentration to improve the performance of the electrodes.^{7,13} One drawback of MoS₂ catalysts is that the number of active sites is limited to edges. If MoS₂ based catalysts are to realize their potential, then there is an urgent need to increase the number of active sites, the

activity of catalytic sites, and the electrical communication between the active sites and the catalyst substrate. Optimization of charge transfer through the utilization of a graphene support, for example, has been demonstrated to substantially improve the kinetics of HER.^{14,15} It has been recently shown that conversion of 2H MoS₂ or WS₂ to 1T phase improves the HER catalytic performance, but the mechanism responsible for the enhancement is presently not completely elucidated.^{16,17} For example, it is unclear if the enhancement in the catalyst

Received: October 1, 2013

Revised: November 12, 2013

Published: November 19, 2013



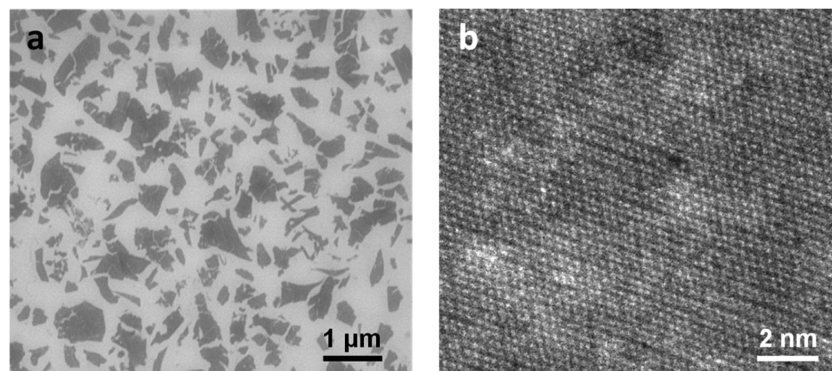


Figure 1. Electron microscope images of chemically exfoliated MoS₂: (a) SEM image of chemically exfoliated MoS₂ nanosheets deposited on SiO₂; (b) HAADF STEM image of chemically exfoliated MoS₂ with octahedral coordination (1T phase). The nanosheets are mostly composed of distorted regions with zigzag chains.

properties is related to increased conductivity of the nanosheets that can facilitate charge transfer kinetics or if the metastable metallic 1T phase of MoS₂ is intrinsically more active. We demonstrate that it is possible to achieve a very high concentration (>80%) of the metallic phase in MoS₂ nanosheets, which leads to a dramatic enhancement in the catalytic activity, most strikingly in improving the Tafel slope. We further show that the catalytic activity of the semiconducting 2H phase of MoS₂ can be improved in terms of decreasing the overpotential via addition of a very small amount of single walled carbon nanotubes (SWNTs). Our results suggest that the catalytic activity of the 1T phase in itself may not be fundamentally different from that of the 2H phase. The activity of the semiconducting 2H MoS₂ phase nanosheets is primarily limited by its high electrical resistance which hinders charge transfer kinetics, but this can be, at least to some degree, mitigated by increasing the conductivity through phase change or doping with SWNT networks that have a very low percolation threshold for conduction.¹⁸

Molybdenum disulfide (MoS₂), a quasi-two-dimensional transition metal dichalcogenide (TMD) having a layered structure, has recently attracted attention due to its novel electronic,^{19,20} optical,^{21,22} optoelectronic,^{23–25} and catalytic¹² properties. The bulk MoS₂ crystal is an indirect band gap semiconductor with an energy gap of 1.29 eV, which consists of several layers of S–Mo–S coupled with weak van der Waals interactions. Each layer itself is built up of an intermediate plane of molybdenum atoms sandwiched between two sulfur atoms with strong covalent bonds between Mo and S. Octahedral (1T phase) and trigonal prismatic (2H and 3R phases) are two coordinations for the molybdenum atoms, and the 2H phase occurs naturally in bulk MoS₂.²⁶ Due to the weak van der Waals interaction between S–Mo–S layers, it is possible to exfoliate the crystal into individual layers that exhibit properties that are dramatically different from the bulk material. Coleman and co-workers²⁷ recently reported liquid-phase exfoliation of bulk MoS₂ powders in appropriate organic solvents with the aid of ultrasonication and centrifugation. It has been previously shown by Joensen et al.²⁸ that Li-intercalated MoS₂ (Li_xMoS₂) can be exfoliated via forced hydration in a form of stable colloidal suspension and strong PL signals can be detected from large area thin films consisting mostly of single layers.²² In addition to the high yield of a single layer in solution, chemical exfoliation through lithium intercalation induces modifications of the crystal structure due to the electron transfer between the lithium compound (*n*-

butyllithium or lithium borohydride) and MoS₂ nanosheets. To accommodate these extra electrons in the d orbitals of the metal atom, calculations²⁹ have demonstrated that octahedral coordination is favorable for d^{x>2}. It results in emergence of metallic property and experimentally coexistence of the two different phases (2H and 1T) within the single layer nanosheet.³⁰

Density functional theory and scanning tunneling microscopy have shown that MoS₂ edges^{11,12} are catalytically active in HER, which has led to optimization of the edge to basal plane ratio using a variety of nanostructures ranging from nanowires to mesoporous architectures.^{31,32} Interestingly, amorphous MoS₂^{33,34} is also catalytically active despite the absence of edges and the role of molybdenum in HER has also been highlighted in studies utilizing molybdenum nitride (MoN), boride (MoB), and carbide (Mo₂C) catalysts.^{35,36} In this work, we aim to provide insight into mechanisms responsible for HER in Mo containing compounds.

For this study, lithium borohydride (LiBH₄) was used as the lithium intercalant to exfoliate bulk MoS₂ powder into single layered nanosheets using the method reported by Kanatzidis et al.³⁷ Monolayered MoS₂ nanosheets as indicated by Raman and PL measurements (Figure S1–3, Supporting Information) obtained from the solid state intercalation reaction can be observed in scanning electron microscope (SEM) images, as shown in Figure 1a. The high resolution scanning transmission electron microscope (STEM) image of the 1T phase is shown in Figure 1b. The indexed diffraction patterns obtained from the 1T and 2H phases match perfectly our previous results for chemically exfoliated MoS₂ prepared via butyllithium.³⁰ The concentration of 1T and 2H phases in the exfoliated products can be detected by X-ray photoelectron spectroscopy (XPS) (see Figure S2, Supporting Information). Deconvolution of the Mo3d and S2p regions in the XPS spectra reveals that the content of the 1T phase in the as-exfoliated monolayers can be as high as 80%, which is significantly higher than exfoliated MoS₂ prepared with *n*-butyllithium (~50%) at room temperature.²²

HER measurements with chemically exfoliated MoS₂ nanosheets on glassy carbon electrodes were carried out using a three-electrode cell with a 0.5 M sulfuric acid electrolyte. 2H phase nanosheets (after annealing) exhibit overpotential values of >250 mV with low current densities. The latter is attributed to low edge concentration due to large lateral dimensions (700–800 nm) and poor conductivity of the nanosheets (Figure S4, Supporting Information). In contrast, chemically

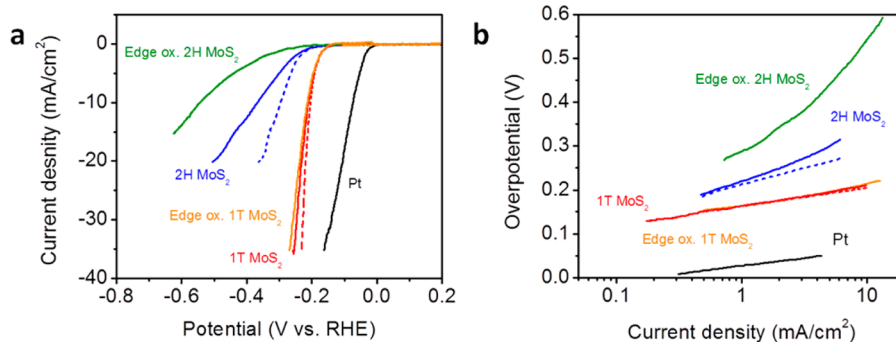


Figure 2. HER activity of exfoliated MoS_2 nanosheets. (a) Polarization curves of 1T and 2H MoS_2 nanosheet electrodes before and after edge oxidation. iR -corrected polarization curves from 1T and 2H MoS_2 are shown by dashed lines. (b) Corresponding Tafel plots obtained from the polarization curves. Tafel slopes of ~ 40 and $75\text{--}85$ mV/dec have been measured for 1T and 2H MoS_2 , respectively. After oxidation, the Tafel slopes of 45 and 186 mV/dec for 1T and 2H MoS_2 , respectively, were obtained.

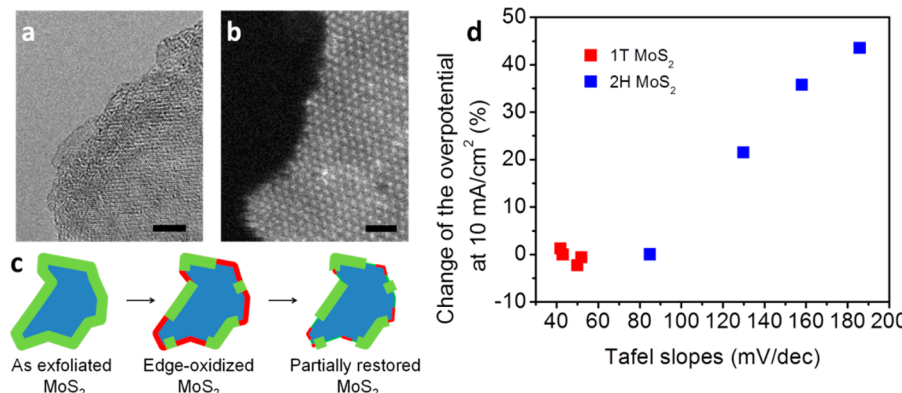


Figure 3. Edge-oxidized MoS_2 nanosheets. High-resolution TEM (a) and HAADF STEM (b) of edge-oxidized MoS_2 nanosheets showing corrugated edges caused by the chemical oxidation. Scale bars: 5 and 1 nm, respectively. (c) Schematic of the oxidation process and partial restoration of the nanosheet edges after several voltammetric cycles. (d) Variation of overpotential at 10 mA cm^{-2} and Tafel slopes for 1T and 2H MoS_2 for as-is samples and after the 1st, 2nd, and 150th voltammetric cycles showing the partial restoration of the HER activity for oxidized 2H MoS_2 . At the opposite, the activity form 1T MoS_2 is virtually not affected by the oxidation.

exfoliated 1T- MoS_2 nanosheets (as-exfoliated) deposited on the glassy carbon electrodes exhibit substantially improved electrocatalytic activity with low overpotentials of ~ 100 mV (Figure 2a). The reaction kinetics are substantially improved in the 1T phase material, as indicated by the exceptionally low Tafel slopes of ~ 40 mV/decade (mV/dec) after iR correction (41–46 mV/dec before the correction) (Figure 2b). The low Tafel slopes indicate that the Volmer–Heyrovsky mechanism¹⁴ is responsible for HER in our case in which the desorption of hydrogen is the rate limiting step. Li et al. also reported a Tafel slope of 40 mV/dec for MoS_2 nanoclusters with high edge concentration deposited on reduced graphene oxide (rGO) due to the improved electronic communication between the active MoS_2 nanoparticles and the highly conductive rGO.¹⁴ Similarly, Lukowski et al. reported a Tafel slope of 40 mV/dec for butyllithium-treated MoS_2 grown on glassy carbon.¹⁷ Such low Tafel slopes have also been reported from amorphous MoS_x deposited by graphene-protected nickel foam¹⁵ on nickel or prepared by cyclic voltamperometry.³³ When converted to the 2H phase, the Tafel slope dramatically increases to above 75–85 mV/dec. The large current density and low Tafel slope demonstrate that the catalytic activity is substantially enhanced in 1T phase MoS_2 .

The exceptionally low Tafel slope values obtained from 1T phase MoS_2 in this study can be attributed to the fact that we took great care to eliminate surface charges that are typically

present on monolayered nanosheets. Upon lithium intercalation, layers of MoS_2 become charged due to the electron transfer between LiBH_4 and MoS_2 . Some of these negative charges react with water during the exfoliation process, but a fraction remain on the nanosheets, rendering them negatively charged. It has been estimated that the quantity of charge remaining after exfoliation per MoS_2 is $\sim 0.15\text{--}0.25$.^{38,39} Charge impurities play a detrimental role in electronics and especially in 2D materials.⁴⁰ We have developed a simple technique that can remove excess charge from the surface of the MoS_2 nanosheets by treating them with iodine dissolved in acetonitrile (see the Supporting Information for details). The removal of some of the negative charge from the nanosheet surface was confirmed by measuring the zeta potential of suspensions before and after the treatment. The drop of the zeta potential from -41 to -27 mV after the iodine treatment indicates that charges are largely suppressed at the surface of the nanosheets (Table S1, Supporting Information). We confirm through XPS that iodine is completely removed after the reaction while the concentration of the 1T phase is not affected (Figure S5, Supporting Information). We find that charge removal leads to an improvement in the overall HER activity of the 1T phase MoS_2 electrodes in terms of lowered overpotential and Tafel slopes (Figure S6, Supporting Information). The removal of charged impurities from the surface of MoS_2 nanosheets facilitates electron transfer between

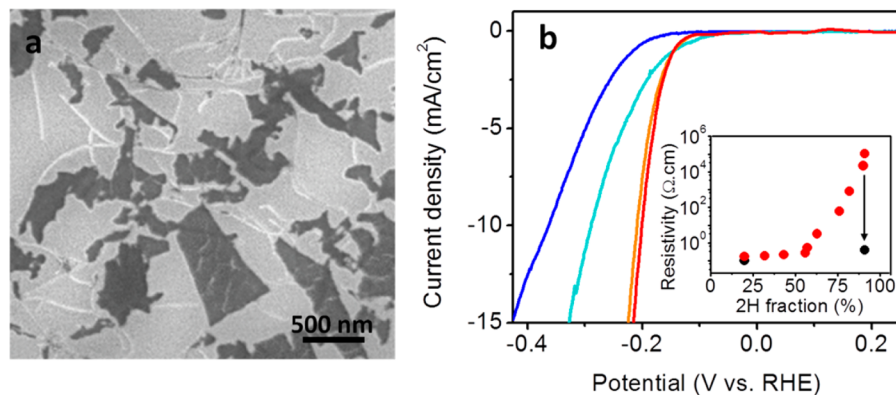


Figure 4. MoS₂/SWNT electrode properties. (a) SEM images of the MoS₂/SWNT hybrids prepared by mixing the SWNT dispersion with the chemically exfoliated MoS₂ solution. (b) Polarization curves of 1T (red and orange) and 2H phase (blue and turquoise) MoS₂ nanosheets with and without SWNTs showing that the addition of SWNTs does not substantially improve the properties of the 1T phase but, in the 2H phase, the SWNTs lead to a decrease in overpotential values (turquoise curve). The inset shows that the resistivity of the chemically exfoliated nanosheets increases with a fraction of 2H phase concentration. However, the addition of SWNTs increases the conductivity of the 2H phase so that it is equivalent to that of the 1T phase.

the nanosheets and the protons in the electrolyte solution during HER.

To investigate the HER mechanism in chemically exfoliated MoS₂ nanosheets, we partially oxidized the nanosheets (see the Supporting Information for details). The reactivity of TMDs toward oxidation is strongly influenced by their electronic structure.⁴¹ Mo-based TMDs have been found to be more stable than their W-based counterpart, and therefore, oxidation of MoS₂ proceeds slowly.⁴¹ The rate of oxidation at low temperature (typically below 100 °C) can be increased by combining water and oxygen.^{42,43} Here MoS₂ nanosheets were partially oxidized over few days in aqueous solution that was saturated with oxygen. It is worth noting that MoS₂ was fully exfoliated and the temperature was kept below 20 °C to ensure a uniform and controlled oxidation. Oxidation was confirmed by the observation of new peaks at 232.4 and 235.5 eV from Mo⁶⁺ 3d_{5/2} and Mo⁶⁺ 3d_{3/2}, respectively, using XPS (Figure S7, Supporting Information). We also measured the concentration of the 1T and 2H phases before and after oxidation and found it to not vary substantially (Figure S7, Supporting Information), which suggests that the oxidation minimally disrupts the atomic arrangement in the basal plane. It has been shown previously that the oxidation of MoS₂ crystals and nanostructures initiates at the edges and propagates into the crystal.^{44,45} Transmission electron microscopy (TEM) confirmed that the edges are highly disordered after oxidation (Figure 3a), while the basal plane of the nanosheets remains preserved, as shown by the scanning transmission electron microscope (STEM) image (Figure 3b). HER measurements on electrodes consisting of edge oxidized 2H phase nanosheets show a dramatically suppressed performance, while the catalytic activity of edge oxidized 1T nanosheets is completely unaffected, as shown in Figure 2 and summarized in Figure 3c. Similar deactivation of the 2H phase of MoS₂ after oxidation has been reported previously and attributed to the edge oxidation.⁴⁶ The absence of any changes in HER with oxidation treatment time in the 1T phase tends to prove that the active sites on chemically exfoliated nanosheets are mainly located in the basal plane and the contribution of the metallic edges on the overall HER is relatively small. Further evidence of the decrease in the catalytic activity of the 2H phase after edge oxidation was provided by impedance spectroscopy. The charge-transfer impedance (Z_f)

was found to dramatically increase for the edge oxidized 2H MoS₂ (Figure S8, Supporting Information) samples. Moreover, we observed that the overall performance of oxidized 2H MoS₂ can be improved upon cycling, which indicates that the catalytic activity from the edges can be partially restored (Figure 3d). The partial restoration of the nanosheets is further confirmed by XPS with a progressive decrease of the Mo⁶⁺ signals between the 1st and the 150th cycle (Figure S7, Supporting Information).

To gain further insight on whether it is the 1T phase that is inherently more catalytically active or if the enhanced performance is due to an increase in conductivity of the nanosheets, we performed additional control experiments in which the conductivity of the 2H phase was increased by adding SWNTs (as shown in the SEM image in Figure 4a and Figure S10, Supporting Information). The addition of ~0.1 wt % SWNTs (slightly above the percolation threshold of SWNT networks) to 2H MoS₂ nanosheets leads to a substantial enhancement in conductivity, achieving values that are comparable to those of pure 1T phase, as shown in the inset of Figure 4b. We confirmed that SWNTs are not active in HER catalysis. However, it can be seen from Figure 4b that the addition of SWNTs to the 2H phase nanosheets has a positive impact on the HER in terms of a decrease in the overpotential to a value that is comparable to that of the 1T phase. Despite this improvement, however, the reaction kinetics are limited by the inefficient adsorption of H⁺ on the basal plane, as indicated by the ~90 mV/dec Tafel slope. These results suggest that the number of accessible active sites on the 2H phase MoS₂ nanosheets has increased, whereas the kinetics of the HER are limited. In contrast, the HER performance of the conducting 1T phase nanosheets is unaffected by the addition of SWNTs, although a slight increase in the Tafel slopes to ~60 mV/dec is observed. The decrease in charge transfer kinetics can also be identified by the larger charge-transfer resistance of 1T MoS₂ and 1T MoS₂/SWNT (Figure S9, Supporting Information). The increase in Tafel slopes in SWNT/MoS₂ hybrids can be attributed to the presence of interfacial resistance between the metallic SWNTs and semiconducting MoS₂ nanosheets in the 2H phase and between semiconducting SWNTs and metallic MoS₂ nanosheets in the 1T phase.

In conclusion, chemically exfoliated MoS₂ nanosheets exhibit excellent electrocatalytic performance for hydrogen evolution. The superior catalytic activity can be attributed to the very high concentration of metallic 1T phase in the chemically exfoliated samples, which substantially improves the charge transfer kinetics of HER. Electrochemical oxidation of the edges leads to a dramatic reduction in catalytic activity for 2H nanosheets, but the catalytic performance is unaffected by oxidation for 1T phase nanosheets, which suggests that the basal plane is catalytically active. The catalytic activity of the 2H phase can be improved by increasing its conductivity through doping with SWNTs. Our results suggest that charge transfer kinetics in metallic MoS₂ is a key parameter for further improving its performance as a catalyst in HER.

Methods. Chemical Exfoliation. Lithium intercalation was done in an Ar-filled glovebox (Vacuum Atmosphere Company glovebox). Bulk MoS₂ was intercalated with lithium via a solvent-free method by reacting MoS₂ powder (0.3 g, Alfa Aesar) with lithium borohydride (0.75 g, Sigma Aldrich) with a 1:2.5 ratio. Both powders were mixed to ensure homogeneity and then heated at 300° under argon. After 3 days, the black powder was immersed in water with a ratio of 1 mg/mL of water. The exfoliation goes fast, and the solution turns completely dark after a few seconds. Sonication was eventually performed for an hour. Lithium cations and non-exfoliated MoS₂ were removed by centrifugation following the same protocol as we recently reported (ref 22).

Physical Characterizations. High angle annular dark field scanning transmission electron microscope (HAADF STEM) imaging was performed using a JEOL JEM-2100F TEM/STEM instrument with double spherical aberration (Cs) correctors (CEOS GmbH, Heidelberg, Germany) at an acceleration voltage of 120 kV. The collecting angle was between 100 and 267 mrad. Scanning electron microscope (SEM) imaging was performed using a Zeiss Sigma Field Emission SEM with an Oxford INCA PentaFETx3 EDS system (model 8100). X-ray photoelectron spectroscopy (XPS) measurements were performed with a Thermo Scientific K-Alpha spectrometer. All spectra were taken using an Al K α microfocused monochromatized source (1486.6 eV) with a resolution of 0.6 eV and a spot size of 400 μ m. Raman spectra were obtained using a Renishaw 1000 system operating at 514 nm (2.41 eV).

Electrochemical Measurements. HER measurements were carried out using a three-electrode cell with a 0.5 M sulfuric acid (H₂SO₄) electrolyte solution. The reactivity of chemically exfoliated MoS₂ toward hydrogen evolution has been systematically measured in hydrogen-saturated and nitrogen-saturated solution. Saturated calomel electrode (Pine Research Instrumentation) and graphite rod (Sigma Aldrich) have been used as reference and counter electrodes, respectively. The reference electrode was calibrated with respect to reversible hydrogen electrode (RHE) using platinum wires as working and counter electrodes. In 0.5 M H₂SO₄, $E_{\text{RHE}} = E_{\text{SCE}} + 0.256$ V. Potential sweeps were taken with a 5 mV/s scan rate using a Pine Bipotentiostat from Pine Research Instrumentation. Electrodes were cycled at least 40 cycles prior to any measurements.

■ ASSOCIATED CONTENT

§ Supporting Information

Details on the iodine treatment, oxidation reaction, Raman and XPS spectroscopy, SEM and size analysis, electrode preparation, UV-vis and photoluminescence, and additional electro-

chemical measurements. This material is available free of charge via the Internet at <http://pubs.acs.org>.

■ AUTHOR INFORMATION

Corresponding Author

*E-mail: manish1@rci.rutgers.edu.

Author Contributions

The manuscript was written through contributions of all authors. All authors have given approval to the final version of the manuscript.

Notes

The authors declare no competing financial interest.

■ ACKNOWLEDGMENTS

M.Chhowalla, D.V., and M.S. acknowledge financial support from NSF DGE 0903661. G.E. acknowledges financial support from NRF Singapore. V.S. acknowledges support from Army Research Office through Contract W911NF-11-1-0171. T.A. acknowledges financial assistance from NSF (CAREER CHE-1004218, DMR-0968937, NanoEHS-1134289, NSF-ACIF, and Special Creativity Grant). T.F. and M.Chen acknowledge partial support from JST-PRESTO “New Materials Science and Element Strategy” and JSPS, Grant-in-Aid for Challenging Exploratory Research (24656028).

■ REFERENCES

- (1) Crabtree, G. W.; Dresselhaus, M. S.; Buchanan, M. V. *Phys. Today* **2004**, *57*, 39–44.
- (2) Greeley, J.; Jaramillo, T. F.; Bonde, J.; Chorkendorff, I.; Nørskov, J. K. *Nat. Mater.* **2006**, *5*, 909–913.
- (3) Lupi, C.; Dell'Era, A.; Pasquali, M. *Int. J. Hydrogen Energy* **2009**, *34*, 2101–2106.
- (4) Evans, D. J.; Pickett, C. J. *Chem. Soc. Rev.* **2003**, *32*, 268–275.
- (5) Okamoto, Y.; Ida, S.; Hyodo, J.; Hagiwara, H.; Ishihara, T. *J. Am. Chem. Soc.* **2011**, *133*, 18034–18037.
- (6) Cobo, S.; Heidkamp, J.; Jacques, P.-A.; Fize, J.; Fourmond, V.; Guetaz, L.; Jousselme, B.; Ivanova, V.; Dau, H.; Palacin, S.; Fontecave, M.; Artero, V. *Nat. Mater.* **2012**, *11*, 802–807.
- (7) Merki, D.; Hu, X. *Energy Environ. Sci.* **2011**, *4*, 3878–3888.
- (8) Helm, M. L.; Stewart, M. P.; Bullock, R. M.; DuBois, M. R.; DuBois, D. L. *Science* **2011**, *333*, 863–866.
- (9) Karunadasa, H. I.; Chang, C. J.; Long, J. R. *Nature* **2010**, *464*, 1329–1333.
- (10) Andreiadis, E. S.; Jacques, P.-A.; Tran, P. D.; Leyris, A.; Chavarot-Kerlidou, M.; Jousselme, B.; Matheron, M.; Pécaut, J.; Palacin, S.; Fontecave, M.; Artero, V. *Nat. Chem.* **2013**, *5*, 48–53.
- (11) Hinnemann, B.; Moses, P. G.; Bonde, J.; Jørgensen, K. P.; Nielsen, J. H.; Horch, S.; Chorkendorff, I.; Nørskov, J. K. *J. Am. Chem. Soc.* **2005**, *127*, 5308–5309.
- (12) Jaramillo, T. F.; Jørgensen, K. P.; Bonde, J.; Nielsen, J. H.; Horch, S.; Chorkendorff, I. *Science* **2007**, *317*, 100–102.
- (13) Laursen, A. B.; Kegnæs, S.; Dahl, S.; Chorkendorff, I. *Energy Environ. Sci.* **2012**, *5*, 5577–5591.
- (14) Li, Y.; Wang, H.; Xie, L.; Liang, Y.; Hong, G.; Dai, H. J. *Am. Chem. Soc.* **2011**, *133*, 7296–7299.
- (15) Chang, Y.-H.; Lin, C.-T.; Chen, T.-Y.; Hsu, C.-L.; Lee, Y.-H.; Zhang, W.; Wei, K.-H.; Li, L.-J. *Adv. Mater.* **2013**, *25*, 756–760.
- (16) Voiry, D.; Yamaguchi, H.; Li, J.; Silva, R.; Alves, D. C. B.; Fujita, T.; Chen, M.; Asefa, T.; Shenoy, V. B.; Eda, G.; Chhowalla, M. *Nat. Mater.* **2013**, *12*, 850–855.
- (17) Lukowski, M. A.; Daniel, A. S.; Meng, F.; Forticaux, A.; Li, L.; Jin, S. *J. Am. Chem. Soc.* **2013**, *135*, 10274–10277.
- (18) Kyrylyuk, A. V.; van der Schoot, P. *Proc. Natl. Acad. Sci. U.S.A.* **2008**, *105*, 8221–8226.
- (19) Yoon, Y.; Ganapathi, K.; Salahuddin, S. *Nano Lett.* **2011**, *11*, 3768–3773.

- (20) Radisavljevic, B.; Radenovic, A.; Brivio, J.; Giacometti, V.; Kis, A. *Nat. Nanotechnol.* **2011**, *6*, 147–150.
- (21) Splendiani, A.; Sun, L.; Zhang, Y.; Li, T.; Kim, J.; Chim, C.-Y.; Galli, G.; Wang, F. *Nano Lett.* **2010**, *10*, 1271–1275.
- (22) Eda, G.; Yamaguchi, H.; Voiry, D.; Fujita, T.; Chen, M.; Chhowalla, M. *Nano Lett.* **2011**, *11*, 5111–5116.
- (23) Yin, Z.; Li, H.; Li, H.; Jiang, L.; Shi, Y.; Sun, Y.; Lu, G.; Zhang, Q.; Chen, X.; Zhang, H. *ACS Nano* **2012**, *6*, 74–80.
- (24) Lee, H. S.; Min, S.-W.; Chang, Y.-G.; Park, M. K.; Nam, T.; Kim, H.; Kim, J. H.; Ryu, S.; Im, S. *Nano Lett.* **2012**, *12*, 3695–3700.
- (25) Mak, K. F.; He, K.; Shan, J.; Heinz, T. F. *Nat. Nanotechnol.* **2012**, *7*, 494–498.
- (26) Wang, Q. H.; Kalantar-Zadeh, K.; Kis, A.; Coleman, J. N.; Strano, M. S. *Nat. Nanotechnol.* **2012**, *7*, 699–712.
- (27) Coleman, J. N.; Lotya, M.; O'Neill, A.; Bergin, S. D.; King, P. J.; Khan, U.; Young, K.; Gaucher, A.; De, S.; Smith, R. J.; Shvets, I. V.; Arora, S. K.; Stanton, G.; Kim, H.-Y.; Lee, K.; Kim, G. T.; Duesberg, G. S.; Hallam, T.; Boland, J. J.; Wang, J. J.; Donegan, J. F.; Grunlan, J. C.; Moriarty, G.; Shmeliov, A.; Nicholls, R. J.; Perkins, J. M.; Grieveson, E. M.; Theuwissen, K.; McComb, D. W.; Nellist, P. D.; Nicolosi, V. *Science* **2011**, *331*, 568–571.
- (28) Joensen, P.; Frindt, R. F.; Morrison, S. R. *Mater. Res. Bull.* **1986**, *21*, 457–461.
- (29) Kertesz, M.; Hoffmann, R. *J. Am. Chem. Soc.* **1984**, *106*, 3453–3460.
- (30) Eda, G.; Fujita, T.; Yamaguchi, H.; Voiry, D.; Chen, M.; Chhowalla, M. *ACS Nano* **2012**, *6*, 7311–7317.
- (31) Chen, Z.; Cummins, D.; Reinecke, B. N.; Clark, E.; Sunkara, M. K.; Jaramillo, T. F. *Nano Lett.* **2011**, *11*, 4168–4175.
- (32) Kibsgaard, J.; Chen, Z.; Reinecke, B. N.; Jaramillo, T. F. *Nat. Mater.* **2012**, *11*, 963–969.
- (33) Merki, D.; Fierro, S.; Vrubel, H.; Hu, X. *Chem. Sci.* **2011**, *2*, 1262–1267.
- (34) Benck, J. D.; Chen, Z.; Kuritzky, L. Y.; Forman, A. J.; Jaramillo, T. F. *ACS Catal.* **2012**, *2*, 1916–1923.
- (35) Chen, W.-F.; Sasaki, K.; Ma, C.; Frenkel, A. I.; Marinkovic, N.; Muckerman, J. T.; Zhu, Y.; Adzic, R. R. *Angew. Chem., Int. Ed.* **2012**, *51*, 6131–6135.
- (36) Vrubel, H.; Merki, D.; Hu, X. *Energy Environ. Sci.* **2012**, *5*, 6136–6144.
- (37) Tsai, H.-L.; Heising, J.; Schindler, J. L.; Kannewurf, C. R.; Kanatzidis, M. G. *Chem. Mater.* **1997**, *9*, 879–882.
- (38) Heising, J.; Kanatzidis, M. G. *J. Am. Chem. Soc.* **1999**, *121*, 11720–11732.
- (39) Golub, A. S.; Zubavichus, Y. V.; Slovokhotov, Y. L.; Novikov, Y. N.; Danot, M. *Solid State Ionics* **2000**, *128*, 151–160.
- (40) Chen, J.-H.; Jang, C.; Adam, S.; Fuhrer, M. S.; Williams, E. D.; Ishigami, M. *Nat. Phys.* **2008**, *4*, 377–381.
- (41) Jaegermann, W.; Schmeisser, D. *Surf. Sci.* **1986**, *165*, 143–160.
- (42) Ross, S.; Sussman, A. *J. Phys. Chem.* **1955**, *59*, 889–892.
- (43) Windom, B. C.; Sawyer, W. G.; Hahn, D. W. *Tribol. Lett.* **2011**, *42*, 301–310.
- (44) Kautek, W.; Gerischer, H. *Surf. Sci.* **1982**, *119*, 46–60.
- (45) Chianelli, R. R.; Ruppert, A. F.; Behal, S. K.; Kear, B. H.; Wold, A.; Kershaw, R. *J. Catal.* **1985**, *92*, 56–63.
- (46) Bonde, J.; Moses, P. G.; Jaramillo, T. F.; Nørskov, J. K.; Chorkendorff, I. *Faraday Discuss.* **2008**, *140*, 219–231.